Dissimilarities between the electronic structure of chemically doped and chemically pressurized iron pnictides from an angle-resolved photoemission spectroscopy study

S. Thirupathaiah, E. D. L. Rienks, H. S. Jeevan, R. Ovsyannikov, E. Slooten, J. Kaas, E. van Heumen, S. de Jong, H. A. Dürr, K. Siemensmeyer, R. Follath, Philipp Gegenwart, M. S. Golden, J. Fink

Angaben zur Veröffentlichung / Publication details:

Thirupathaiah, S., E. D. L. Rienks, H. S. Jeevan, R. Ovsyannikov, E. Slooten, J. Kaas, E. van Heumen, et al. 2011. "Dissimilarities between the electronic structure of chemically doped and chemically pressurized iron pnictides from an angle-resolved photoemission spectroscopy study." *Physical Review B* 84 (1): 014531. https://doi.org/10.1103/physrevb.84.014531.

Dissimilarities between the electronic structure of chemically doped and chemically pressurized iron pnictides from an angle-resolved photoemission spectroscopy study

S. Thirupathaiah,[1] E. D. L. Rienks,[1] H. S. Jeevan,[2] R. Ovsyannikov,[1] E. Slooten,[3] J. Kaas,[3] E. van Heumen,[3] S. de Jong,[3,4] H. A. Dürr,[1,4] K. Siemensmeyer,[1] R. Follath,[1] P. Gegenwart,[2] M. S. Golden,[3] and J. Fink[1,5]

[1]*Helmholtz-Zentrum Berlin, Albert-Einstein-Strasse 15, D-12489 Berlin, Germany*

[2]*I. Physikalisches Institut, Georg-August-Universität-Göttingen, D-37077 Göttingen, Germany*

[3]*Van der Waals-Zeeman Institute, University of Amsterdam, 1018 XE Amsterdam, The Netherlands*

[4]*Pulse Institute and Stanford Institute for Energy and Materials Science, SLAC National Accelerator Laboratory, Menlo Park, California 94025, USA*

[5]*Leibniz-Institute for Solid State and Materials Research Dresden, P.O. Box 270116, D-01171 Dresden, Germany*

(Received 24 November 2010; revised manuscript received 17 May 2011; published 29 July 2011)

We have studied the electronic structure of $EuFe_2As_{2-x}P_x$ using high-resolution angle-resolved photoemission spectroscopy. Upon substituting As with the isovalent P, which leads to chemical pressure and to superconductivity, we observe a nonrigid-band-like change of the electronic structure along the center of the Brillouin zone (BZ) in the form of an orbital and k_z-dependent increase or decrease in the size of the hole pockets near the $\Gamma - Z$ line. The diameter of the Fermi surface cylinders at the BZ corner which form electron pockets, increases at K and changes in a nonmonotonous way at X. This is in stark contrast to p- and n-type doped iron pnictides where, on the basis of ARPES experiments, a more rigid-band-like behavior has been proposed. These findings indicate that there are different ways in which the nesting conditions can be reduced causing the destabilization of the antiferromagnetic order and the appearance of the superconducting dome.

DOI: 10.1103/PhysRevB.84.014531 PACS number(s): 74.70.Xa, 71.20.−b, 74.25.Jb, 79.60.−i

I. INTRODUCTION

The discovery of high T_c superconductivity in ferropnictides[1] has attracted a great deal of attention not only because of the high superconducting transition temperatures T_c up to 55 K but also because of the complex phase diagrams. Starting from the antiferromagnetic (AF) metallic parent compounds, superconductivity can be induced in various ways: by chemical doping, i.e., introducing electrons or holes, by pressure, or by chemical pressure. An example of the latter route is to substitute the smaller yet formally isovalent P for As in the Ba122 compound.[2] The designation A122 is used to refer to the AFe_2As_2 systems where A = Ca, Sr, Ba, or Eu. All these methods lead to similar phase diagrams in which the AF order is suppressed with increasing distance from the parent compound and a superconducting dome appears. The similarity of the phase diagrams hints at a common mechanism for this behavior. In a more itinerant picture, which is still under debate, these phase diagrams are explained in terms of decreasing nesting conditions between hole pockets in the center and electron pockets at the corner of the Brillouin zone (BZ).[3] The similarity of the phase diagrams may indicate that in all cases the nesting conditions are reduced in the same way; i.e., the evolution of the electronic structure as a function of the distance to the parent compound is the same. On the other hand, the application of doping, pressure, or chemical pressure may be taking different routes to reach the same destination, inducing differing changes to the electronic structure.

In previous angle-resolved photoemission spectroscopy (ARPES) studies,[4–8] a doping-induced reduction of the nesting conditions has been reported: for n-type doped systems such as $BaFe_{2-x}Co_xAs_2$, a gradual decrease (increase) of the size of the hole (electron) pockets has been detected. For p-type doped systems such as $Ba_{1-x}K_xFe_2As_2$, the opposite behavior has been observed. On the basis of these results, a doping-induced shift of the Fermi level E_F in a rigid-band-like electronic structure has been proposed.[7,8] Theoretically, the ARPES results have been supported by density functional calculations (DFT) in the virtual crystal approximation and using super cells.[8,9] There is not, however, unanimity on the point of doping leading to a simple shift of the chemical potential. Recent super cell DFT calculations of different dopants (among other Co) on the Fe site indicated the formation of localized states leading to an isovalent substitution instead of chemical doping.[10]

$Ba(Eu)Fe_2As_{2-x}P_x$ (see Refs. 2 and 11) is an ideal system to study the evolution of the electronic structure as a function of chemical pressure. In the Ba122 compound, P substitution has led to superconductivity with a T_c up to 30 K.[2] In the Eu122 system, the AF order of the Fe ions is also suppressed by P substitution and the Eu ions order antiferromagnetically below 18 K. At higher P concentrations, however, the Eu moments order ferromagnetically, which limits the superconducting dome to a narrow range between $x = 0.3$ and 0.4.[12] To the best of our knowledge, no ARPES investigations have been performed on these systems. Recently, a series of articles on the electronic structure of $BaFe_2As_{2-x}P_x$ compounds using the de Haas-van Alphen (dHvA) effect have been published.[13–16] Powerful as they are, these dHvA measurements do have the drawback that, due to the short mean free path of the hole carriers, it is difficult to identify and analyze the hole-like Fermi surfaces in the substituted compounds.

In this contribution, we present a systematic study of the evolution of the electronic structure of the chemically pressurized system $EuFe_2As_{2-x}P_x$ using high-resolution ARPES to reveal the dispersion of bands parallel and perpendicular to the Fe layers. We obtain information on the orbital character of the states near the Fermi level. Moreover, we provide results on the size of the hole and the electron Fermi surfaces and the

related nesting conditions as a function of P substitution. We observe nonrigid-band-like shifts of bands related to the hole and electron pockets. Therefore, our data show that differing routes can and are taken to reach superconductivity in the ferropnictides: upon aliovalent substitution there are signs for a Fermi level shift in a more or less rigid-band structure, whereas isovalent substitution—chemical pressure—gives a strongly nonrigid-band-like evolution.

II. EXPERIMENTAL DETAILS

Single crystals of $EuFe_2As_2$ and the P substituted compounds were grown in Göttingen using the Sn-flux and the Bridgman (without Sn flux) method, respectively.[17] The AF transition temperature T_N for the Fe^{2+} moments in the parent compound was determined to be about 190 K while Eu^{2+} moments order antiferromagnetically below $T_N = 18$ K. A narrow superconducting dome with a maximum transition temperature $T_c = 29$ K has been observed around $x = 0.4$.[12] In Fig. 1, we present susceptibility data of a $EuFe_2As_{1.68}P_{0.32}$ single crystal to show that the sample has a superconducting transition temperature $T_c \approx 22$ K. Below $T_N = 18$ K, the Eu^{2+} moments exhibit antiferromagnetic order. A ferromagnetic order is detected at higher P concentrations, which suppresses superconductivity. ARPES measurements were carried out at the Helmholtz-Zentrum Berlin synchrotron radiation facility BESSY II using the UE112-PGM2 beam line and "1^3"-ARPES end station equipped with a Scienta R4000 analyzer. The total energy resolution was set between 5 and 7 meV, while the angular resolution was 0.2° (0.3°) parallel (perpendicular) to the analyzer slit. High-symmetry points of the BZ are denoted by $\Gamma = (0,0,0)$, $Z = (0,0,1)$, $X = (1/2,1/2,0)$, and $K = (1/2,1/2,1)$ in units of $(2\pi/a, 2\pi/a, 2\pi/c)$, where a and c are the tetragonal lattice constants of $EuFe_2As_{2-x}P_x$. This is a coordinate system parallel to the Fe–As direction. For the discussion of the orbital character, we will use a basis that is aligned parallel to the nearest-neighbor Fe–Fe direction. In this way, it is easier to compare the data with calculations presented in Ref. 18. We note that this second coordinate system is rotated by 45° around the k_z axis compared to that used in our previous work.[8,19] All measurements were performed below 20 K if not otherwise stated. Further experimental details have been published previously.[19]

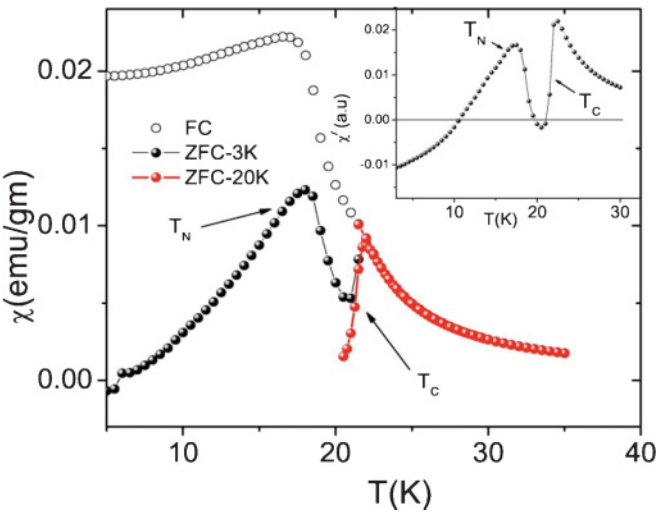

FIG. 1. (Color online) DC susceptibility data of $EuFe_2As_{1.68}P_{0.32}$. We show measurements under the conditions of zero field cooling (ZFC) and field cooling (FC) for an applied field of 50 Oe parallel to the ab plane. The inset shows the ac susceptibility.

III. RESULTS

Figure 2 shows representative ARPES data of $EuFe_2As_{1.56}P_{0.44}$, a slightly over-substituted compound. The map displayed in Fig. 2(a) shows an ellipsoidal Fermi surface (FS) formed by an electron pocket [see Fig. 2(b)] around the X point, the intensity of which is strongly reduced along the $\Gamma - X$ line. This reduction might be related to matrix element effects suppressing the intensity along a mirror plane for specific photon polarizations.[8] The intensity reduction along the $\Gamma - X$ line, however, remains for p-polarized light and for geometries free of mirror plane effects. According to Ref. 18, the Fermi surface at X should have yz and xy character perpendicular and parallel to the $\Gamma - X$ line, respectively. Both should be visible in our geometry for s-polarized light. Thus the xy states would have to be strongly suppressed by matrix element effects other than

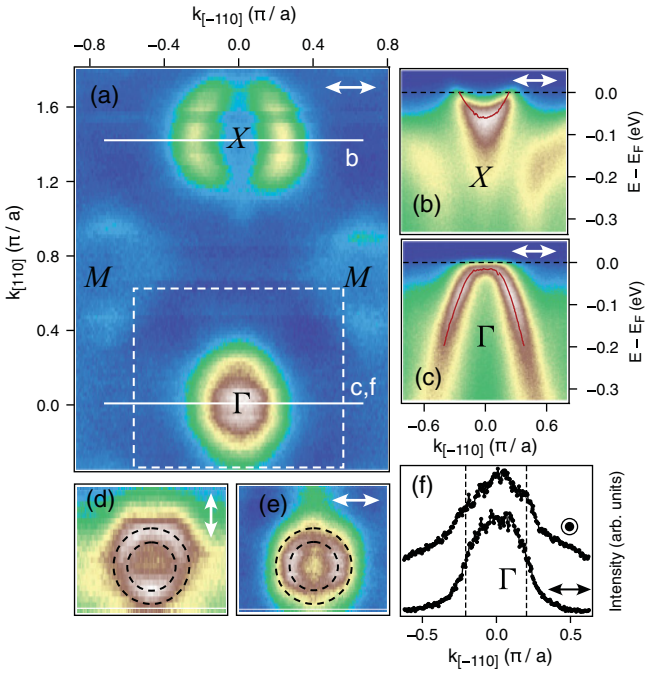

FIG. 2. (Color online) ARPES data of $EuFe_2As_{1.56}P_{0.44}$ taken with a photon energy $h\nu = 93$ eV. (a) Fermi surface map along $\Gamma - X$ symmetry line measured with s-polarized light (indicated by a double arrow). Solid white lines indicate the directions of the cuts shown in (b), (c), and (f). (b) and (c) Energy distribution maps near X and Γ, respectively. Solid red lines connect the maxima obtained by least squares fits to momentum distribution curves (MDC). Energy distribution curve fit results are shown in the immediate vicinity of the high-symmetry points. (d) and (e) Constant energy contours 50 meV below E_F for two different polarizations in the k range indicated by the white dashed rectangle in (a). Dashed circles are guides to the eye. (f) MDCs near Γ at E_F for s and p polarization.

the polarization selection rules. This view is supported by ARPES measurements on cuprates[20] and by matrix element calculations for ferropnictides.[6] Consequently, we state that the visible part of the FS of the electron pocket near the X point has yz character. Next, we discuss the spectral weight in Fig. 2(a) near Γ, which results from hole bands, the top of which are close to E_F [see Fig. 2(c)]. Polarization-dependent constant energy contours at 50 meV below E_F shown in Figs. 2(d) and 2(e) indicate two almost degenerate hole pockets with an asymmetric intensity distribution around Γ, which can be nicely explained by the calculations of Ref. 18 in terms of xz/yz bands. The inner (outer) pocket shows more intensity for the yz (xz) arcs perpendicular (parallel) to $\Gamma - X$ for s (p)-polarized light. In the momentum distribution curves shown in Fig. 2(f), we detect a further outermost hole pocket at Γ, highlighted by dashed lines, for p- but not for s-polarized photons. Contrary to the inner two pockets, this third pocket clearly crosses the Fermi level. From the low intensity and from the fact that these states are only weakly dependent on k_z (see below), we tentatively assign this hole pocket to xy states. The polarization dependence could be explained by a small matrix element for the odd xy states and an admixture of even $x^2 - y^2$ states. Summarizing the results derived from Fig. 2, our data on the orbital character of the states close to E_F at Γ and X are compatible with the theoretical results presented in Ref. 18.

To elucidate the 3D nature of the electronic structure, we have measured $h\nu$-dependent ARPES data at the center and at the corner of the BZ (see Fig. 3). An inner potential of 15 eV has been used to calculate the k_z values from $h\nu$ with the c values reported in Ref. 11. The Γ, Z, X, and K points are indicated by dashed lines. Along the $\Gamma - Z$ direction, we compare data taken with two different polarizations, so as to enable the extraction of important information regarding the orbital character of the states near E_F. For s-polarized light, in this geometry, for $k_{[-110]} = 0$ we can detect only

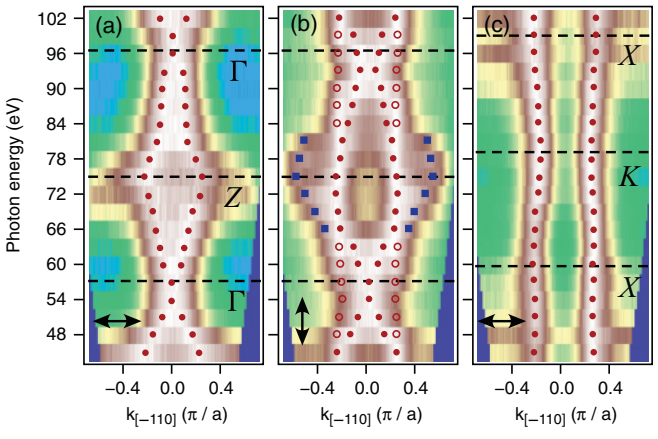

FIG. 3. (Color online) ARPES Fermi surface maps of $EuFe_2As_{1.56}P_{0.44}$ in the $k_{[001]} - k_{[-110]}$ plane. Actually, the photon-energy dependence of the intensity is shown. (a) and (b) Data near the $\Gamma - Z$ line taken with s- and p-polarized light, respectively. (c) Data near the corner of the BZ measured with s-polarized light. The symbols indicate the band dispersion having different orbital character: open (closed) circles predominantly xy (xz/yz) character, closed squares predominantly z^2 character.

odd states relative to the $\Gamma - X$ mirror plane and therefore the k_z dispersive band in Fig. 3(a) has yz character. For p-polarized photons, we are sensitive to even states, which have xz, $x^2 - y^2$, and z^2 character. Thus, we identify the inner slightly dispersing Fermi cylinders with the almost degenerate xz/yz bands, different from our previous assignment.[8] The next largest Fermi cylinder shows little k_z dispersion and is assigned to xy states, made visible in this geometry by the admixture of even $x^2 - y^2$ states. In agreement with our previous results,[8] we assign the outermost Fermi cylinder, which carries significant spectral weight near the Z point, to z^2 states. As is to be expected, the k_z dispersion is large for orbitals not lying in the Fe plane and small for in-plane orbitals. The data near $k_x, k_y = 0$ indicate a considerably large k_z dispersion, i.e., a larger three-dimensionality when compared to the nonsubstituted compound. At the zone corner, we observe only a small k_z dispersion of the Fermi cylinder.

Analogous measurements as those shown in Figs. 2 and 3 have been performed for the P concentrations $x = 0, 0.28$, and 0.32. In Fig. 4, we present ARPES data of the parent compound $EuFe_2As_2$ recorded at $T = 220$ K near the high-symmetry points Z, Γ, K, and X using a photon energy $h\nu = 75$ eV for Z and K, and $h\nu = 96$ eV for Γ and X. These data were

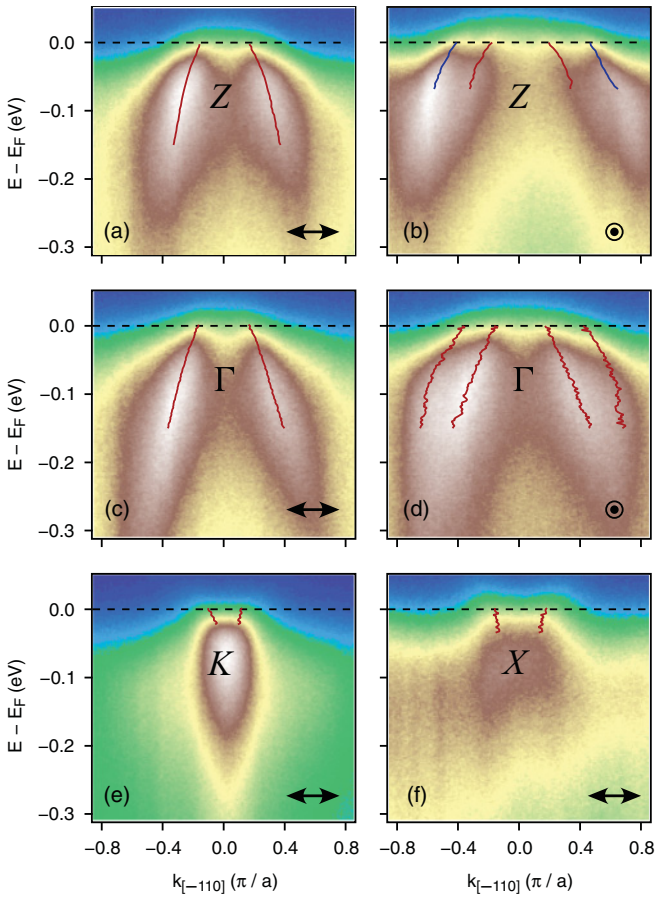

FIG. 4. (Color online) ARPES energy distribution maps near the high-symmetry points Γ, X, Z, and K of the parent compound $EuFe_2As_2$ taken in the paramagnetic state at $T = 220$ K. The data near Z and Γ were recorded using both s- and p-polarized photons. The data near K and X were obtained using s-polarized photons.

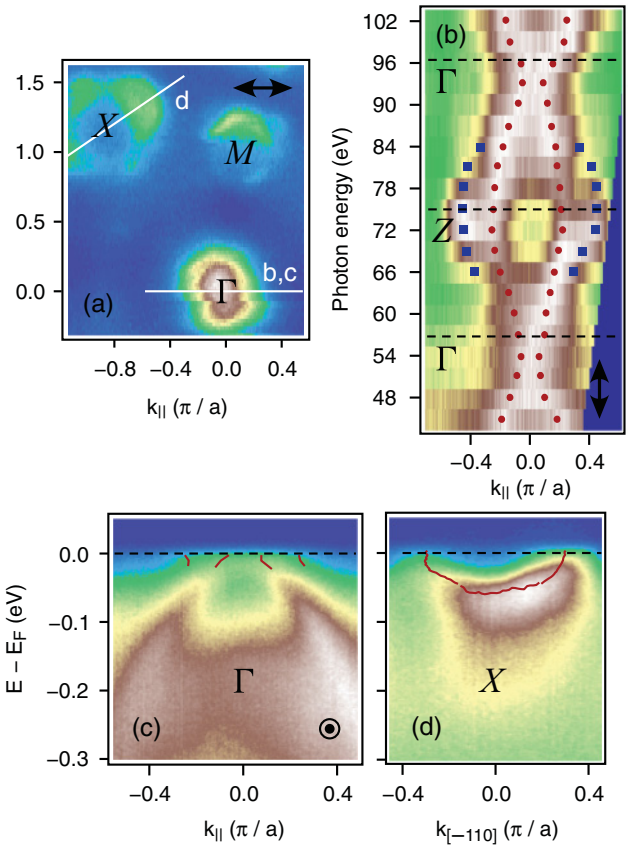

FIG. 5. (Color online) ARPES of $EuFe_2As_{1.72}P_{0.28}$. (a) A Fermi surface map for $k_z = 0$. The k_z dispersion at the zone center is given in (b). (c) and (d) Energy distribution maps taken near the Γ and X points, respectively.

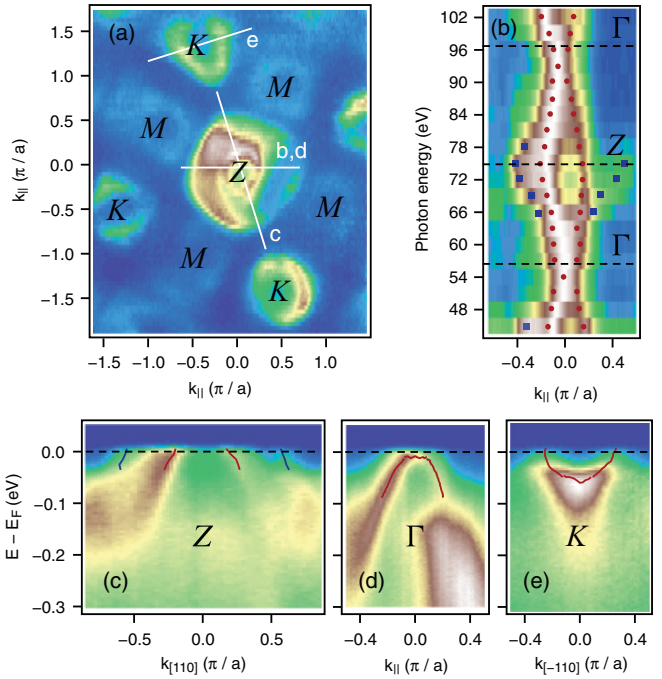

FIG. 6. (Color online) ARPES of $EuFe_2As_{1.68}P_{0.32}$. (a) A Fermi surface map for $k_z = 1$. The white lines indicate the directions of the measurements shown in (b)–(e). (b) The k_z dispersion at the zone center. (c), (d), and (e) EDMs taken near the Z, Γ, and K points, respectively. The data were taken with circularly polarized photons.

measured in the paramagnetic state of $EuFe_2As_2$ in order to obtain information on the electronic structure in a state in which no back-folding and hybridization of the bands due to the antiferromagnetic order has occurred. In this way we can compare the changes of possible nesting conditions in the entire substitution range. Near Z and Γ we obtain—for s-polarized photons—one hole pocket, while for p-polarized photons two hole pockets are observed. Near K and X, one electron pocket is detected for s-polarized photons. The band dispersion overlaid on the data is derived from a fit of the momentum distribution curves (MDCs) using a superposition of Lorentzians.

Figure 5 presents ARPES data of $EuFe_2As_{1.72}P_{0.28}$. Fermi surface maps parallel (for $k_z = 0$) and perpendicular (in the zone center) to the Fe layers and energy distribution maps (EDMs) at the Γ and X points are displayed. In Fig. 5(a) we see a clear feature at the M point, probably caused by a (2×1) ordering of the Eu atoms at the surface. A similar ordering of the Ba atoms has been recently described for the Ba122 compound.[21]

Finally, in Fig. 6 we present ARPES data of a superconducting $EuFe_2As_{1.68}P_{0.32}$ crystal. Fermi surface maps parallel and perpendicular to the Fe layers, and EDMs near the Z, Γ, and K points are displayed.

In order to derive the k_F values for the hole and electron pockets at the high-symmetry points Γ, Z, X, and K, we have evaluated the MDCs at the Fermi level near these points. In Fig. 7, we present such MDCs for various P concentrations together with a least squares fit from which we derive the k_F values labeled by symbols already used in Fig. 3. Note that different photon polarizations have been used for the measurements, and therefore bands with different orbital character are obtained. The assignment was already performed during the discussion of the data shown in Figs. 2 and 3. We also point out that all these MDCs were recorded for crystals in the paramagnetic tetragonal phase, i.e., for small P concentrations above the Néel temperature.

In Fig. 8(a), we present the k_F values along the $k_{[-110]}$ direction for the high-symmetry points Γ, Z, X, and K as a function of P substitution. These k_F values are calculated from the average of the absolute values of the positive and negative k_F values derived from the MDCs shown in Fig. 7. At Γ the size of the xz/yz hole pockets as well as that of the xy pocket decrease with x. At Z, the size of the z^2 hole pocket is for $x \leqslant 0.32$ almost constant and then increases when going to $x = 0.44$, whereas the almost degenerate $xy, xz/yz$ hole pockets slightly increase. The size of the electron pockets at X increases between $x = 0$ and $x = 0.28$ and then decreases for $x = 0.44$. The size of the electron pocket at K increases with x.

We contrast the k_F values for $EuFe_2As_{2-x}P_x$ with analogous values [see Fig. 8(b)] for the chemically doped system $BaFe_{2-x}Co_xAs_2$, which were taken from the data presented in Ref. 8. In this case, both the hole pockets at Γ and at Z

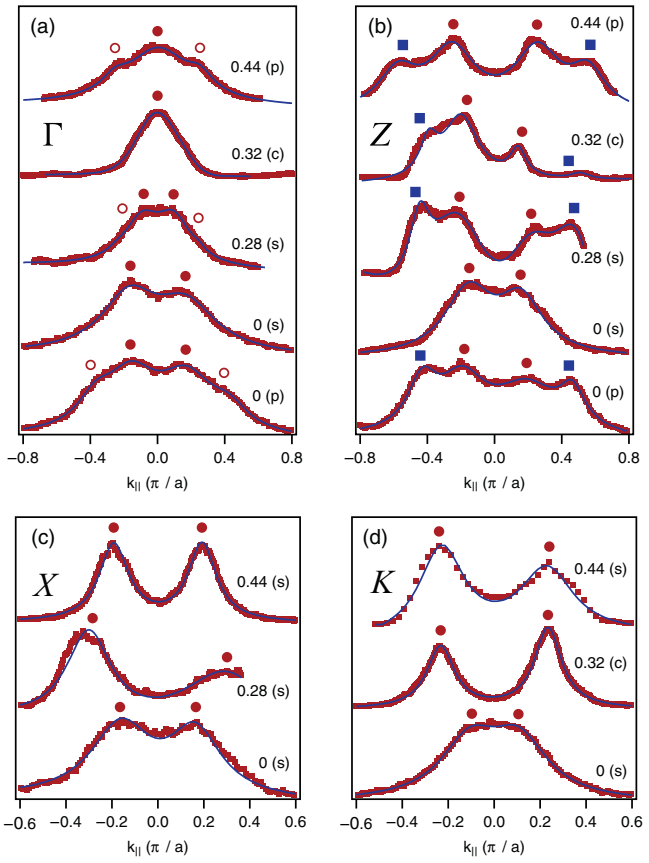

FIG. 7. (Color online) Momentum distribution curves at the Fermi level integrated over 10 meV near the high-symmetry points Γ, Z, X, and K for $EuFe_2As_{2-x}P_x$. The P concentration x increasing in all cases from bottom to top are given in the individual panels. The data taken with s, p, and circularly polarized photons are labeled with (s), (p), and (c), respectively. Dots (red): measured data; solid (blue) line: result from a least squares fit. Maxima derived from these fits are marked by symbols which are the same as described in the legend of Fig. 3, indicating the orbital character of the bands.

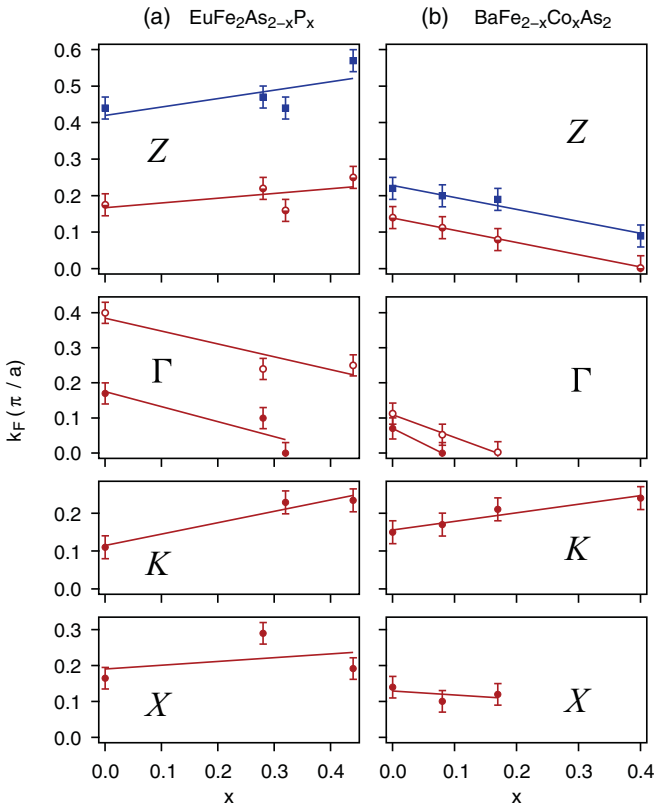

FIG. 8. (Color online) Fermi vectors plotted as a function of doping/substitution concentrations at Z, Γ, K, and X. (a) Isovalently substituted (chemically pressurized) system $EuFe_2As_{2-x}P_x$. (b) Aliovalently substituted (electron doped) $BaFe_{2-x}Co_xAs_2$. The assignment of the symbols to the orbital character is the same as described in the legend of Fig. 3. Half-filled circles indicate xy and xz/yz character. The solid lines are least-squares fits assuming a linear dependence of k_F on x (see text).

decrease with increasing Co concentration while the electron pocket increases.

IV. DISCUSSION

First we discuss the evolution of the electronic structure of $EuFe_2As_{2-x}P_x$ and $BaFe_{2-x}Co_xAs_2$ as a function of substitution concentration. We start this discussion by pursuing the total charge of the systems as a function of x. For $k_F \gg dk_F$ and for a 2D electronic structure there is a linear relationship between the concentration-dependent changes of the total number of charge carriers $dn_{e,h}/dx$ and the concentration dependence of the Fermi vector dk_F/dx:

$$dn_{e,h}/dx = 2\pi k_F (dk_F/dx)/S_{BZ}, \qquad (1)$$

where $S_{BZ} = (2\pi/a)^2$ is the area of the BZ.

Using the k_F data of $EuFe_2As_{2-x}P_x$ presented in Fig. 8(a), the slight increase of the hole pockets at Z and the stronger decrease of those at Γ is roughly compensated by the increase of the electron pockets at K. This is compatible with a charge-neutral replacement of the As atoms by P, as is to be expected for isovalent substitution.

For $BaFe_{2-x}Co_xAs_2$, the linear changes of the k_F values with increasing x are in agreement with Eq. (1). Thus, the solid lines shown in Fig. 8(b) are based on a physical model in which Eq. (1) is used, approximating the 3D Fermi surface with that of a cylinder, taking a k_F value which is an average of that observed experimentally for $k_z = 0$ and 1. In this way, we derive an increase of the total charge of 0.7 electrons per Co atom. This value is close to the value of 1 derived in the work of Ref. 7. In spite of the fact that we have not measured the Fermi surfaces for the full 3D Brillouin zone, we can conclude that there is significant charge transfer from the Co dopants to the Fe-derived bands.

For the system $BaFe_{2-x}Co_xAs_2$, several other ARPES studies have been published,[4–6] all indicating a rigid-band-like behavior upon n-type doping with Co (and for p-type doping by replacement of Ba by K). Thus, all these ARPES data support part of the DFT calculations both in the virtual crystal approximation[8] and using super cells.[9] On the other hand, it would be interesting to perform similar ARPES measurements on Ni or Cu "doped" $BaFe_2As_2$ to study the interesting

question when a localization of the extra 3*d* electrons occurs as predicted in Ref. 10.

While the data on $BaFe_{2-x}Co_xAs_2$ indicate *n*-type doping by the Co atoms in a more or less rigid-band system, in $EuFe_2As_{2-x}P_x$ a nonrigid-band evolution of the electronic structure is detected. Along the central line of the Brillouin zone (Γ-Z), the size of the hole pockets decrease, increase, or remain constant with increasing P concentration, whereas in the corner of the BZ the size of the electron pockets increases at K and shows a nonmonotonous dependence at X. The nonrigid-band evolution of electronic structure is probably related to a change of the crystal field splitting of the Fe 3*d* states upon substitution of the larger As ions by the smaller isovalent P ions, thus changing the pnictogen height above the Fe layers. As a consequence, the solid lines in Fig. 8(a) are merely a guide to the eye, using a linear relationship that is not based on a physical model. A recent structural study on $BaFe_2As_{2-x}P_x$ (Ref. 22) has shown that the pnictogen height dependence on the substitution level is significantly different for As and P. This fact can possibly explain the complicated changes of the k_F values for the different Fe 3*d* orbitals as a function of x.

A comparison between the data for the unsubstituted systems in Figs. 8(a) and 8(b) further reveals that the k_F values for the hole-like states in the Eu compound are significantly larger. The apparently larger number of holes in the Eu parent compound is not understood at present.

Next, we discuss the nesting conditions in the two systems. Using again the approximation of cylindrical Fermi surfaces, the strength of the interband nesting conditions is determined by the similarity of the k_F values of the hole and the electron pockets presented in Fig. 8. Close to optimal doping (maximal T_c), we observe a closing of the xz/yz hole pockets at $k_z = 0$, for both the P and the Co substituted system. This would mean that at optimal doping the nesting condition is strongly reduced compared to that in the parent compound and possibly makes the nesting between the electron pockets more important. In this way it would be possible to understand doping-dependent changes of the symmetry of the superconducting order parameter,[23] e.g., from $s^{\pm}$ to d. A similar scenario was described in Ref. 24. On the other hand, we see that the deterioration of the degree of nesting between the electron and hole states at nonzero k_z values is much less pronounced: the hole-like bands persist at higher substitution levels at $k_z = 1$, which means they are available for nesting even well above the optimal "doping" concentration. Summarizing this part of the discussion: (i) despite the differing routes to reach the electronic structure pertaining to optimal doping the P-substituted and Co-doped compounds share significantly weakened nesting conditions between hole and electron Fermi surfaces; (ii) in the "over-doped" composition, nesting remains important for the P case at nonzero k_z values, while for Co doping the xz/yz hole pockets are filled for $x \geqslant 0.4$ even at Z. This means that in the latter system nesting between the xz/yz bands is no longer possible. This could explain why superconductivity disappears for Co concentrations $x \geqslant 0.4$. For $EuFe_2As_{2-x}P_x$, the situation is less clear for high P concentrations.

During our manuscript preparation, we noticed a similar dHvA study on $BaFe_2(As_{0.37}P_{0.63})_2$ in which an enhanced nesting for the superconducting compound in comparison to the fully substituted compound was derived.[25] We point out that in these measurements only one instead of three hole pockets have been detected and therefore on the basis of these data it is difficult to conclude on the nesting conditions.

V. CONCLUSIONS

In summary, we have performed high-resolution ARPES studies on $EuFe_2As_{2-x}P_x$ in order to reveal the nature of the electronic structure as a function of x. The results are compared with analogous data of the electron doped $BaFe_{2-x}Co_xAs_2$ system. We conclude that the evolution of electronic structure upon substitution of As by P in $EuFe_2As_2$, which leads to chemical pressure, is nonrigid-band-like in nature. On the other hand, for the aliovalently substituted system $BaFe_{2-x}Co_xAs_2$, we see more signs compatible with a shift of E_F in a rigid-band-like electronic structure. Our findings are supporting the importance of nesting conditions for the understanding of the phase diagram, the appearance of superconductivity and the pairing symmetry of the order parameter in ferropnictide compounds.

After submission of our manuscript, an analogous ARPES study on the P-substituted Ba122 system had appeared.[26]

ACKNOWLEDGMENTS

Financial support by the DFG through SPP1458 and from FOM (NWO) is gratefully acknowledged.

[1] Y. Kamihara, T. Watanabe, M. Hirano, and H. Hosono, J. Am. Chem. Soc. **130**, 3296 (2008).
[2] S. Jiang, H. Xing, G. Xuan, C. Wang, Z. Ren, C. Feng, J. Dai, Z. Xu, and G. Cao, J. Phys. Condens. Matter **21**, 382203 (2009).
[3] I. I. Mazin, D. J. Singh, M. D. Johannes, and M. H. Du, Phys. Rev. Lett. **101**, 057003 (2008).
[4] W. Malaeb *et al.*, J. Phys. Soc. Jpn. **78**, 123706 (2009).
[5] K. Terashima *et al.*, Proc. Natl. Acad. Sci. USA **106**, 7330 (2009).
[6] Y. Zhang *et al.*, Phys. Rev. B **83**, 054510 (2011).
[7] V. Brouet *et al.*, Phys. Rev. B **80**, 165115 (2009).
[8] S. Thirupathaiah *et al.*, Phys. Rev. B **81**, 104512 (2010).
[9] A. S. Sefat, R. Jin, M. A. McGuire, B. C. Sales, D. J. Singh, and D. Mandrus, Phys. Rev. Lett. **101** (2008).
[10] H. Wadati, I. Elfimov, and G. A. Sawatzky, Phys. Rev. Lett. **105**, 157004 (2010).
[11] Z. Ren, Q. Tao, S. Jiang, C. Feng, C. Wang, J. Dai, G. Cao, and Z. Xu, Phys. Rev. Lett. **102**, 137002 (2009).
[12] H. S. Jeevan, D. Kasinathan, H. Rosner, and P. Gegenwart, Phys. Rev. B **83**, 054511 (2011).
[13] S. Kasahara *et al.*, Phys. Rev. B **81**, 184519 (2010).

[14]J. G. Analytis, C. M. J. Andrew, A. I. Coldea, A. McCollam, J.-H. Chu, R. D. McDonald, I. R. Fisher, and A. Carrington, Phys. Rev. Lett. **103**, 076401 (2009).
[15]A. I. Coldea, C. M. J. Andrew, J. G. Analytis, R. D. McDonald, A. F. Bangura, J.-H. Chu, I. R. Fisher, and A. Carrington, Phys. Rev. Lett. **103**, 026404 (2009).
[16]H. Shishido *et al*., Phys. Rev. Lett. **104**, 057008 (2010).
[17]H. S. Jeevan, Z. Hossain, D. Kasinathan, H. Rosner, C. Geibel, and P. Gegenwart, Phys. Rev. B **78**, 052502 (2008).
[18]S. Graser, T. A. Maier, P. J. Hirschfeld, and D. J. Scalapino, New J. Phys. **11**, 025016 (2009).
[19]J. Fink *et al*., Phys. Rev. B **79**, 155118 (2009).
[20]D. S. Inosov *et al*., Phys. Rev. Lett. **99**, 237002 (2007).
[21]E. van Heumen *et al*., Phys. Rev. Lett. **106**, 027002 (2011).
[22]M. Rotter, C. Hieke, and D. Johrendt, Phys. Rev. B **82**, 014513 (2010).
[23]M. A. Tanatar, J.-P. Reid, H. Shakeripour, X. G. Luo, N. Doiron-Leyraud, N. Ni, S. L. Bud'ko, P. C. Canfield, R. Prozorov, and L. Taillefer, Phys. Rev. Lett. **104**, 067002 (2010).
[24]K. Kuroki, H. Usui, S. Onari, R. Arita, and H. Aoki, Phys. Rev. B **79**, 224511 (2009).
[25]J. Analytis, J.-H. Chu, R. McDonald, S. C. Riggs, and I. Fisher, Phys. Rev. Lett. **105**, 207004 (2010).
[26]T. Yoshida *et al*., Phys. Rev. Lett. **106**, 117001 (2011).